Quasi-static electric field computation using axial Green function method for moving boundaries

Junhong Jo[1], Hong-Kyu Kim[2], Chang-Seob Kwak[2], and Do Wan Kim[1]

[1]Department of Mathematics, Inha University, Incheon 22212, South Korea
[2]Korea Electrotechnology Research Institute, Changwon 51543, South Korea

Moving boundary takes place frequently in electric devices such as circuit breakers. The computational domain for quasi-static electric field caused by moving boundaries that change in time and accordingly it is important to be able to continuously construct the spacial discretization in an efficient way for accurate calculation. The axial Green function method must be available for this kind of problems. The benefit for this selection lies in the easier way to construct axial lines in complicated domains compared to grid or mesh generator in FDM or FEM. Not only the automatic axial line generation is fast and easy to implement but also it is efficient because we can generate them individually and independently in each subdomain into which the whole computational domain is partitioned.

***Index Terms*—Moving boundary, circuit breaker, axial line generator, axial Green function method.**

I. Introduction

Electric fields in a domain with moving boundaries can be viewed as quasi-static field when the speed of the moving boundary is low enough compared to the electromagnetic wave speed scale. The axisymmetric circuit breaker illustrated in Fig. 1 yields the complicated computational domain which consists of regions of grey colors and the shield of green color. In real situation, the nozzle and arcing contacts, on which we have $V = 100$ as an enforced voltage, move leftward. Instead, for simplicity, we make the fixed arcing contact boundary moving right, which is located at the axis of rotation (dotted line) and on which we put $V = 0$. In addition, the shield (green region) and the enclosure isolated in the light grey region are also moving right at the same speed. On the enclosure, we also have $V = 0$ as the boundary voltage. The other relevant boundary conditions and permittivities are shown in Fig. 1 in detail. The emphasis in this paper is laid on how we calculate the quasi-static electric field efficiently in the varying domain triggered by the moving boundaries. For this purpose, we apply the axial Green function method(AGM) to this moving boundary problem. AGMs developed so far has turned out to be successful in accurate computation of the axisymmetric electromagnetic fields [1] in complicated domains with different permittivities and Neumann boundaries [2]. The aim of AGM is to solve some sort of physically important problems governed by partial differential equations in complicated domains using one-dimensional Green functions, for instance, the general elliptic equation, the Stokes flow[3], and the convection-dominated diffusion equation[4]. AGMs use the axial lines as a discrete skeleton like grid or mesh in FDM or FEM. One more thing to emphasize is that arbitrary refinements of axial lines are available in AGMs. In this paper, since moving boundary is the keyword, we focus on how to automatically generate the axial lines in a computational domain of AGM. Indeed, the electric field computation of the circuit breaker is inevitable for its optimal design. As an application to this, we investigate the reliability on a gas circuit breaker based on the AGM solutions for the quasi-static electric field resulting from the moving boundaries.

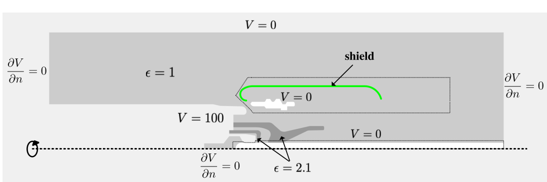

Fig. 1. Circuit breaker with boundaries moving: the moving boundaries are the fixed arcing contact ($V = 0$) at the axis of rotation (dotted line), the enclosure ($V = 0$) hollow in the middle, and the shield (slim green region). There are two fixed dotted-polygonal regions at the bottom and the middle, respectively, which contains moving parts, the arcing contact(bottom) and the enclosure hollow including the shield(middle).

II. Axial line generator

Since AGM for quasi-static solutions of the moving boundary problem needs to generate the axial lines automatically and efficiently as well, it is necessary to implement the refined axial lines independently and individually in specified subdomains, particularly in the subdomains containing moving boundaries. In our case, around the fixed arcing contact boundary on the axis of rotation, the enclosure, and the shield, we install three rectangular subregions to which the moving regions entirely belong. In AGMs, the axial lines can be independently generated in each subregion[2]. In fact, it becomes an extraordinary advantage in numerical methods without doubt. Let Ω be a schematic computational domain in 2D as illustrated in Fig. 2. Each boundary $\Gamma^{(i)}$ of Ω is defined as a set of ordered points $\mathbf{x}_k^{(i)}$ for $k = 0, 1, \cdots, n$ together with the straight line segments $\overline{\mathbf{x}_{k-1}^{(i)}\mathbf{x}_k^{(i)}}$ for $k = 1, \cdots, n$. We call $\overline{\mathbf{x}_{k-1}^{(i)}\mathbf{x}_k^{(i)}}$ the boundary segment. It means that the line segments defining a boundary of the domain have a consistent orientation, i.e., $\Gamma^{(1)}$ is counterclockwise whereas $\Gamma^{(2),(3)}$ is clockwise in Fig. 2. At first, we take a bounding box of the

978-1-5386-6425-4/18/$31.00 ©2018 IEEE

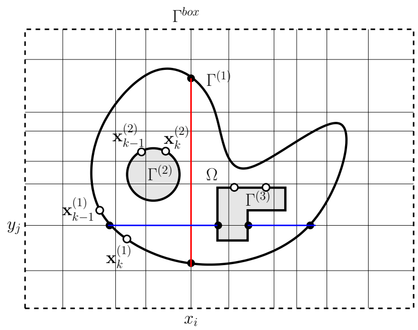

Fig. 2. Schematic diagram for axial line generator: Ω is a domain inside $\Gamma^{(1)}$ and outside $\Gamma^{(2),(3)}$ where $\Gamma^{(i)}$ is the boundaries of Ω, and Γ^{box} is a bounding box(dotted rectangular box) taken so as to contain Ω. $\overline{\mathbf{x}_{k-1}^{(i)}\mathbf{x}_k^{(i)}}$ is a straight line segment called the boundary segment defining discrete boundaries.

entire domain Ω which is denoted by Γ^{box} as shown in Fig. 2. Assume that the coordinates x_i's and y_j's are placed along the horizontal and vertical sides of the bounding box Γ^{box}, respectively. Each line segment belonging to the rectangular domain bounded by Γ^{box} whose x-coordinate(or y-coordinate) is x_i(or y_j) is denoted by $\bar{Y}^{x_i}$(or $\bar{X}^{y_j}$). All we need to generate axial lines begins with finding its intersection points with all boundaries, the black dots on the boundaries as shown in Fig. 2, to obtain the maximal axial lines like the blue line and the red line in Fig. 2.

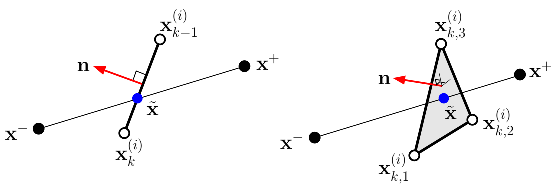

(a) 2D boundary (b) 3D boundary

Fig. 3. Basic algorithm to find the boundary points intersecting with a given line segment $\overline{\mathbf{x}^-\mathbf{x}^+}$ inside Γ^{box}.

The key algorithm to do this is to efficiently find these intersecting points. We consider the 2D case first. Assume that $L_k^{(i)} \equiv \overline{\mathbf{x}_{k-1}^{(i)}\mathbf{x}_k^{(i)}}$ stands for the k-th boundary segment of $\Gamma^{(i)}$ with unit normal vector $\mathbf{n}$ and $\overline{\mathbf{x}^-\mathbf{x}^+}$ is a given line segment which will be replaced with $\bar{Y}^{x_i}$ or $\bar{X}^{y_i}$. Define the unit vector $\mathbf{q}$,

$$\mathbf{q} = \frac{\mathbf{x}^+ - \mathbf{x}^-}{\|\mathbf{x}^+ - \mathbf{x}^-\|}, \tag{1}$$

and we can obtain the orthogonal projector onto the hyperplane Π passing through the origin in 2D, which is perpendicular to the vector $\mathbf{q}$, such that

$$P_\Pi = I - \mathbf{q}\,\mathbf{q}^T, \tag{2}$$

where I is 2×2 identity matrix, $\mathbf{q}$ is viewed as 2×1 matrix, and $\mathbf{q}^T$ is the transpose of $\mathbf{q}$. Therefore, P^Π is 2×2 matrix in 2D case. In order to calculate the intersection point $\tilde{\mathbf{x}}$ between $L_k^{(i)}$ and $\overline{\mathbf{x}^-\mathbf{x}^+}$ in Fig. 3(a), the first thing that we have to know is whether they meet or not. This can be done by investigating the two images, $\mathbf{y}_{k-1}^{(i)} \equiv \mathbf{x}_{k-1}^{(i)} - \mathbf{x}^-$ and $\mathbf{y}_k^{(i)} \equiv \mathbf{x}_k^{(i)} - \mathbf{x}^-$. The image line segment $\overline{\mathbf{y}_{k-1}^{(i)}\mathbf{y}_k^{(i)}}$ contains the origin $\mathbf{0}$ if and only if the extended line of $\overline{\mathbf{x}^-\mathbf{x}^+}$ in the direction of $\mathbf{q}$ always meets the line segment $L_k^{(i)}$ at some point $\hat{\mathbf{x}}$. At this moment, we introduce the following useful fact whose proof is done in Appendix A.

Lemma. Assume that $\mathbf{a}_i$ is m-dimensional vector for $i = 1, 2, \cdots, n$. Then, $\|\mathbf{a}_1 + \cdot + \mathbf{a}_n\| = \|\mathbf{a}_1\| + \cdots + \|\mathbf{a}_n\|$ if and only if $\mathbf{a}_i = \gamma_i \sum_{j=1}^n \mathbf{a}_j$ for $\gamma_i \geq 0$ satisfying $\gamma_1 + \cdots + \gamma_n = 1$.

Either one of the following can occur:

1) $\|\mathbf{y}_k^{(i)} - \mathbf{y}_{k-1}^{(i)}\| < \|\mathbf{y}_k^{(i)}\| + \|\mathbf{y}_{k-1}^{(i)}\|$,
2) $\|\mathbf{y}_k^{(i)} - \mathbf{y}_{k-1}^{(i)}\| = \|\mathbf{y}_k^{(i)}\| + \|\mathbf{y}_{k-1}^{(i)}\| > 0$,
3) $\|\mathbf{y}_k^{(i)}\| = \|\mathbf{y}_{k-1}^{(i)}\| = 0$.

The statement of 1) above is equivalent to the fact that the origin $\mathbf{0}$ does not belong to the line segment $\overline{\mathbf{y}_{k-1}^{(i)}\mathbf{y}_k^{(i)}}$. This implies that, in case of 1), there is no such $\hat{\mathbf{x}}$. In case of 2), however, there exists unique $\hat{\mathbf{x}}$ which is represented as follows using the Lemma above and similarity due to the orthogonal projection:

$$\hat{\mathbf{x}} = \frac{l_k}{l}\,\mathbf{x}_{k-1}^{(i)} + \frac{l_{k-1}}{l}\,\mathbf{x}_k^{(i)}, \tag{3}$$

where $l_{k-1} = \|\mathbf{y}_{k-1}^{(i)}\|$, $l_k = \|\mathbf{y}_k^{(i)}\|$, and $l = l_{k-1} + l_k > 0$. However, it should be noted that $\hat{\mathbf{x}}$ cannot be the point $\tilde{\mathbf{x}}$ in Fig. 3(a) unless $\hat{\mathbf{x}}$ is placed on the line segment $\overline{\mathbf{x}^-\mathbf{x}^+}$. Therefore, we have to check out the following index

$$\alpha = \frac{(\hat{\mathbf{x}} - \mathbf{x}^-) \bullet \mathbf{q}}{\|\mathbf{x}^+ - \mathbf{x}^-\|}. \tag{4}$$

If $0 \leq \alpha \leq 1$, then we can conclude that $\hat{\mathbf{x}}$ is the unique intersecting point, i.e., $\tilde{\mathbf{x}} = \hat{\mathbf{x}}$. In case of 3), $L_k^{(i)}$ entirely belongs to $\overline{\mathbf{x}^-\mathbf{x}^+}$, so that we skip this case, i.e., do nothing in this case. Lastly, we attach a tag at every boundary point $\tilde{\mathbf{x}}$

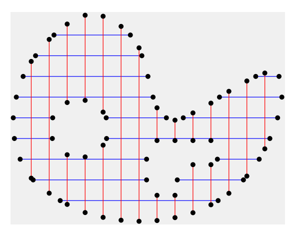

Fig. 4. The boundary points and the corresponding maximal axial lines in Ω calculated by the axial line generator.

by calculating $\beta = \mathbf{q} \bullet \mathbf{n}$ which is not zero in case of 2). For example, if $\beta < 0$, then $\tilde{\mathbf{x}}$ has $'+'$ as a tag. Otherwise($\beta < 0$), we assign $'-'$ to $\tilde{\mathbf{x}}$. The tags, $'+'$ and $'-'$, mean inward-the-domain and outward-the-domain, respectively. Accordingly, for a given $\overline{\mathbf{x}^-\mathbf{x}^+}$, find all intersecting points $\tilde{\mathbf{x}}$ with all the boundary segments and the line segment from the $'+'$-tagged to the consecutive $'-'$-tagged $\tilde{\mathbf{x}}$ becomes an maximal axial line we want to generate as seen in Fig. 2. Practically, it is more efficient to sort all the found boundary points on $\overline{\mathbf{x}^-\mathbf{x}^+}$ with respect to the value α's. With this procedure described so far, we generate uniformly distributed axial lines illustrated in Fig. 4 on the domain drawn in Fig. 2.

On the other hand, in case of 3D as in Fig. 2(b), all boundaries can be described in terms of a set of oriented triangles endowed with unit outward normal vectors $\mathbf{n}$. Similar to (2), we consider the orthogonal projector P_Π onto the hyper surface Π containing the origin $\mathbf{0}$ and orthogonal to the unit vector $\mathbf{q}$ made from (1) in 3D. The projected image of the k-th triangle T_k on (i)-th boundary with vertices, $\mathbf{x}_{k,1}^{(i)}$, $\mathbf{x}_{k,2}^{(i)}$, and $\mathbf{x}_{k,3}^{(i)}$, under the orthogonal projector P_Π becomes a triangle T_k^Π on Π with vertices, $\mathbf{y}_{k,s}^{(i)} \equiv P_\Pi(\mathbf{x}_{k,s}^{(i)} - \mathbf{x}^-)$ for $s = 1, 2, 3$. We call this T_k^Π the projected triangle of T_k on Π. Analogously, the origin $\mathbf{0}$ is contained in T_k^Π if and only if the extended line of $\overline{\mathbf{x}^-\mathbf{x}^+}$ in the direction of $\mathbf{q}$ always meets the triangle T_k at some point $\hat{\mathbf{x}}$. In 3D, either the following inequality holds:

$$\begin{aligned} &\|\mathbf{y}_{k,1}^{(i)} \times \mathbf{y}_{k,2}^{(i)} + \mathbf{y}_{k,2}^{(i)} \times \mathbf{y}_{k,3}^{(i)} + \mathbf{y}_{k,3}^{(i)} \times \mathbf{y}_{k,1}^{(i)}\| \\ &< \|\mathbf{y}_{k,1}^{(i)} \times \mathbf{y}_{k,2}^{(i)}\| + \|\mathbf{y}_{k,2}^{(i)} \times \mathbf{y}_{k,3}^{(i)}\| + \|\mathbf{y}_{k,3}^{(i)} \times \mathbf{y}_{k,1}^{(i)}\|, \end{aligned} \tag{5}$$

or

$$\begin{aligned} &\|\mathbf{y}_{k,1}^{(i)} \times \mathbf{y}_{k,2}^{(i)} + \mathbf{y}_{k,2}^{(i)} \times \mathbf{y}_{k,3}^{(i)} + \mathbf{y}_{k,3}^{(i)} \times \mathbf{y}_{k,1}^{(i)}\| \\ &= \|\mathbf{y}_{k,1}^{(i)} \times \mathbf{y}_{k,2}^{(i)}\| + \|\mathbf{y}_{k,2}^{(i)} \times \mathbf{y}_{k,3}^{(i)}\| + \|\mathbf{y}_{k,3}^{(i)} \times \mathbf{y}_{k,1}^{(i)}\| > 0, \end{aligned} \tag{6}$$

unless

$$\|\mathbf{y}_{k,1}^{(i)} \times \mathbf{y}_{k,2}^{(i)}\| + \|\mathbf{y}_{k,2}^{(i)} \times \mathbf{y}_{k,3}^{(i)}\| + \|\mathbf{y}_{k,3}^{(i)} \times \mathbf{y}_{k,1}^{(i)}\| = 0. \tag{7}$$

Here, it is worth noting that the left hand side of (5) or (6) is the area of the projected triangle T_k^Π by means of the identity

$$\begin{aligned} &\|(\mathbf{y}_{k,2}^{(i)} - \mathbf{y}_{k,1}^{(i)}) \times (\mathbf{y}_{k,3}^{(i)} - \mathbf{y}_{k,1}^{(i)})\| \\ &= \|\mathbf{y}_{k,1}^{(i)} \times \mathbf{y}_{k,2}^{(i)} + \mathbf{y}_{k,2}^{(i)} \times \mathbf{y}_{k,3}^{(i)} + \mathbf{y}_{k,3}^{(i)} \times \mathbf{y}_{k,1}^{(i)}\|. \end{aligned} \tag{8}$$

Among three cases (5)-(7), only the case of (6) has the unique intersecting point $\hat{\mathbf{x}}$ between T_k^Π and the extended line of $\overline{\mathbf{x}^-\mathbf{x}^+}$ since $\mathbf{0} \in T_k^\Pi$ and the area of T_k^Π is not zero from (6) and (8). Applying the Lemma to the case of (6), the point $\hat{\mathbf{x}}$ is calculated in the following form,

$$\hat{\mathbf{x}} = \frac{S_1}{S}\,\mathbf{x}_{k,1}^{(i)} + \frac{S_2}{S}\,\mathbf{x}_{k,2}^{(i)} + \frac{S_3}{S}\,\mathbf{x}_{k,3}^{(i)}, \tag{9}$$

where $S_1 = \frac{1}{2}\|\mathbf{y}_{k,2}^{(i)} \times \mathbf{y}_{k,3}^{(i)}\|$, $S_2 = \frac{1}{2}\|\mathbf{y}_{k,3}^{(i)} \times \mathbf{y}_{k,1}^{(i)}\|$, $S_3 = \frac{1}{2}\|\mathbf{y}_{k,1}^{(i)} \times \mathbf{y}_{k,2}^{(i)}\|$, and S is the area of the projected triangle T_k^Π and $S = S_1 + S_2 + S_3 > 0$. In order that $\tilde{\mathbf{x}} = \hat{\mathbf{x}}$, we again use (4) to determine whether $0 \le \alpha \le 1$ or not as done in 2D.

After finding all boundary points intersecting with every $\bar{X}^{y_j}$ and $\bar{Y}^{x_i}$ using the above strategy, we search all cross points between them on every maximal axial line generated. The procedure in the above can be systematically conducted in both 2D and 3D. The detailed calculations are much easier and simpler than those in the grid or mesh generations of FDM or FEM. Therefore, the auto-axial line generator is made based on these processes and applied directly to the moving boundary problem in this paper.

III. Circuit Breaker with Moving Boundaries

Since AGM for quasi-static solutions of the moving boundary problem in a circuit breaker needs to generate the axial lines automatically and efficiently as well, it is necessary to regenerate the axial lines at each time independently and individually in two fixed dotted-polygonal regions at the bottom and the middle of Fig. 1. These regions cover the fixed arcing contact boundary on the axis of rotation and the enclosure together with the shield whose zoomed-in parts are depicted at the bottom and top panels, respectively, in Fig. 5. Axial line

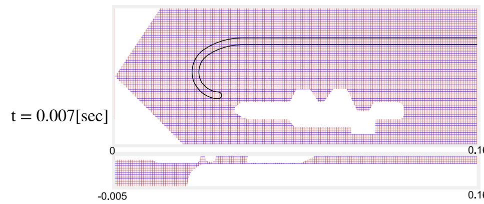

Fig. 5. At time $t = 0.007$[sec] as a representative, axial lines generated in two fixed regions with moving boundaries inside. The moving speed of the moving parts is assumed to be 4[m/sec]. Each of three panels consists of two specified regions, upper region(the enclosure together with the shield) and lower region(the fixed arcing contact).

construction in the entire domain at each time is also available but it must be more time consuming than the strategy we employ here. The strategy specifying two regions for moving boundaries is more efficient because we can use a fixed axial lines generated at the beginning on the complement domain except two regions. The axial lines individually generated on the two specified regions may be non-matching to the fixed axial lines on the complement domain along the contacting boundaries, but it can be solved by the method proposed in [2]. We assume that the constant speed of moving parts is 4[m/sec].

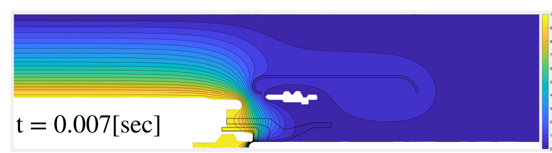

Fig. 6. Axisymmetric electric potential at time $t = 0.007$ as the specified boundaries move right in a constant speed 4[m/sec].

We take 50 moving slots from the initially given configuration ($t = 0$). As a result of generating axial lines and computing the potentials, the total number of cross points about axial lines ranges from 126,401 to 127,439, and about 15 minutes are elapsed for all the 50 slots. The calculated potential when $t = 0.007$[sec] is shown in Fig. 6 on the axial lines generated in the manner of Fig. 5. Of interest are the spots where the highest gradients of the potentials happen at different position as the moving boundaries move right. The maximum electric field intensities when $t = 0, 0.007, 0.014$ take place at $(0.3100 \times 10^{-1}, 0.1000 \times 10^{-1})$, $(0.3400 \times 10^{-1}, 0.9481 \times 10^{-2})$, and $(0.6300 \times 10^{-1}, 0.9766 \times 10^{-2})$, respectively, on the arcing contact. The corresponding maximum electric strengths are calculated to be 0.2870×10^6, 0.5836×10^5, and 0.9550×10^4, respectively. These results are fully attributed to the easy and fast auto-axial-line generator as proposed in the previous section.

IV. Analysis of Capacitive Current Interrupting Performance of GCB

SF_6 gas circuit breakers(GCB) are widely installed in high voltage power networks because of high dielectric performance and powerful interrupting capability. One of the most important duties of a circuit breaker is the capacitive current interruption [5]. If the fault accident occurs, the electric contacts are separated after current interruption and the transient recovery voltage(TRV) is applied between the contact electrodes. If the withstanding voltage is higher than TRV, then circuit breaker successfully clears the fault condition. However, in the opposite case, a dielectric breakdown occurs and circuit breaker fails to interrupt the fault condition. The withstanding voltage V_{bd} is a function of the gas pressure(or density) and electric field intensity:

$$V_{bd} = a\,\frac{\rho^b}{E}, \tag{10}$$

where E is the local electric field intensity, ρ is the gas density, and we take $b = 0.7$ while a is a secure scaling factor depending on the circuit breaker shape. To know ρ and E

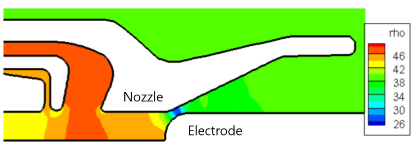

Fig. 7. The SF_6 density ρ when electrode escapes from the nozzle region.

in (10), we have to calculate the transient variation of these values with respect to the moving boundaries. The former is calculated with FVM[6] and the latter is computed with the AGM equipped with axial line generator. Fig. 7 shows ρ

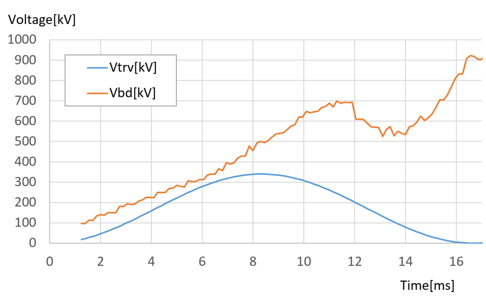

Fig. 8. Comparison of TRV (V_{trv}) and withstanding voltage (V_{bd}).

when the electrode or arcing contact is just pulling out the nozzle throat. Fig. 8 shows the comparison of the TRV and withstanding voltage V_{bd} which is calculate by (10), in which V_{bd} forms greater than TRV. This means that the current GCB model can endure the dielectric stress caused by TRV and thus we can predict successful interruption.

V. Conclusion

The axial line generating is so easy that we can calculate the electromagnetic fields in complicated domains and even in moving boundary problems like circuit breaker. In 3D, this is very strong advantage compared to other methods like finite difference methods, finite elements methods, etc. In practice, axial lines of good quality are automatically generated so as to solve problems in arbitrary domain. If we know the moving region in advance, then it is more convenient to generate axial lines for computing the moving boundary problems. By just updating the new axial lines only in the bounding box of the moving subdomain that we know a priory, we can save time for computing. Therefore, generating axial lines at each time is not a burden for the moving boundary problems any more if using the Axial Green function Methods. Practically, based on the accurate AGM solutions for the quasi-static electric fields under the moving boundaries in a gas circuit breaker model, the withstanding voltage can be successfully calculated to investigate its durability.

Appendix A
Proof of Lemma

It is obvious that if $\mathbf{a}_i = \gamma_i \sum_{j=1}^n \mathbf{a}_j$ for $\gamma_i \geq 0$ satisfying $\gamma_1 + \cdots + \gamma_n = 1$, then $\|\mathbf{a}_1 + \cdot + \mathbf{a}_n\| = \|\mathbf{a}_1\| + \cdots + \|\mathbf{a}_n\|$. For the proof of sufficiency, we prove the Lemma by using the mathematical induction. First, we assume that $\|\mathbf{a}_1 + \mathbf{a}_2\| = \|\mathbf{a}_1\| + \|\mathbf{a}_2\|$. Then, squaring both sides gives the identity $\mathbf{a}_1 \bullet \mathbf{a}_2 = \|\mathbf{a}_1\|\,\|\mathbf{a}_2\|$. This means that $\mathbf{a}_1 = \gamma\,\mathbf{a}_2$ for some $\gamma \geq 0$ if $\|\mathbf{a}_2\| \geq \|\mathbf{a}_1\|$. Therefore, we can conclude that $\mathbf{a}_2 = \frac{1}{1+\gamma}(\mathbf{a}_1 + \mathbf{a}_2)$ and $\mathbf{a}_1 = \frac{\gamma}{1+\gamma}(\mathbf{a}_1 + \mathbf{a}_2)$. Next, we assume that the sufficiency is true in case of $n-1$ members. For n members, we have to prove the sufficiency. Under the assumption that

$$\|\mathbf{a}_i + \cdots + \mathbf{a}_n\| = \|\mathbf{a}_i\| + \cdots + \|\mathbf{a}_n\|, \tag{11}$$

we observe the following relationships for any $i = 1, \cdots, n$:

$$\|\mathbf{a}_i + \cdots + \mathbf{a}_n\| = \|\mathbf{a}_i + \sum_{j\neq i}^{n} \mathbf{a}_j\| \leq \|\mathbf{a}_i\| + \|\sum_{j\neq i}^{n} \mathbf{a}_j\|$$

$$\leq \|\mathbf{a}_i\| + \sum_{j\neq i}^{n} \|\mathbf{a}_j\| = \|\mathbf{a}_i + \cdots + \mathbf{a}_n\|, \tag{12}$$

where the last equality comes from our assumption. In fact, since the second inequality in (12) must be equality, we have $\mathbf{a}_i = \gamma_i\,(\mathbf{a}_1 + \cdots + \mathbf{a}_n)$ for some $\gamma_i \geq 0$, $\sum_{k\neq i}^n \mathbf{a}_k = \hat{\gamma}\,(\mathbf{a}_1 + \cdots + \mathbf{a}_n)$ for some $\hat{\gamma} \geq 0$, and $\gamma_i + \hat{\gamma} = 1$, applying two member case. Therefore, from the assumption for n members, we can conclude that $\gamma_1 + \cdots + \gamma_n = 1$. The proof is done.

Acknowledgment

The authors would like to thank KERI. D.W.Kim is also supported by NRF under Grant(2017R1A4A1014735).

References

[1] W. Lee, H.-K. Kim, and D.W. Kim, *Axial green function method for axisymmetric electromagnetic field computation,* IEEE Trans. Magn., vol. 53, no. 6, Art. no. 7206504, 2017.
[2] J. Jo, H.-K. Kim, and D.W. Kim, *Electric field computations using axial Green function method on refined axial lines,* IEEE Trans. Magn., vol. 54, no. 3, Art. no. 7201604, 2018.
[3] S. Jun and D. W. Kim, *Axial Green's Function Method for Steady Stokes Flow in Geometrically Complex Domains,* J. Comput. Phys., vol. 230, pp. 2095-2124, 2011.
[4] W. Lee and D. W. Kim, *Localized Axial Green's Function Method for the Convection-Diffusion Equations in Arbitrary Domains,* J. Comput. Phys., vol. 275, pp. 390-414, 2014.
[5] H.-K. Kim, K.-Y. Park, C.-H. Im, and H.-K. Jung, *Optimal Design of Gas Circuit Breaker for Increasing the Small Current Interruption Capacity,* IEEE Trans. Magn., vol. 39, no. 3, pp. 1749-1752, 2003.
[6] Y. Zhao and D.E. Winterbone, *The finite volume flic method and its stability analysis,* Int. J. Mesh. Sci., vol. 37, pp. 1147-60, 1995.